Full title

Disease-attenuated pneumococcal biosynthesis gene mutants invade the mucosal epithelium and induce innate immunity

Short title

Epithelial-pneumococcal interactions

Caroline M. Weight[1*±], Gabriele Pollara[1], Modupeh Betts[1], Roberta Ragazzini[2], Elisa Ramos-Sevillano[3], Jesús Reiné[4], Matthew Whelan[1], José Afonso Guerra-Assunção[1], Michael Connor[5], Paola Bonfanti[1,2], Clare Jolly[1], Mahdad Noursadeghi[1], Daniela M. Ferreira[4], Jeremy S. Brown[3], Robert S. Heyderman[1±]

[1]Research Department of Infection, Division of Infection and Immunity, UCL London, UK

[2]Francis Crick Institute, London, UK

[3]Department of Respiratory Medicine, UCL, London, UK

[4]Oxford Vaccine Group, University of Oxford, Oxford and Clinical Sciences, Liverpool School of Tropical Medicine, Liverpool, UK

[5]Chromatin and Infection, Institut Pasteur, France

*Current address Biomedical and Life Sciences, Faculty of Health and Medicine, Lancaster University, UK

±Corresponding Authors: Dr Caroline M. Weight and Professor Robert S. Heyderman

Email: c.weight@lancaster.ac.uk and r.heyderman@ucl.ac.uk

Word Count:

Introduction, results, discussion, methods = 3500

ABSTRACT

Nasopharyngeal colonisation by *Streptococcus pneumoniae* is characterised by bacterial adherence to epithelial cells, microinvasion and innate immune activation. Previously, we have shown two serotype 6B *S. pneumoniae* mutant strains affecting bacterial metabolism (Δ*proABC/pia* and Δ*fhs/pia*) colonise humans and mice, but in a murine disease model do not cause invasive infection. Here, we explore whether *S. pneumoniae* epithelial microinvasion and the induction of innate immune responses persist despite disease attenuation.

We show that under serum stress, these biosynthesis gene mutations had a broad but different impact on pneumococcal virulence gene expression, oxidative stress regulation, and purine and carbohydrate metabolism genes. However, although these mutations did not attenuate microinvasion in human challenge and epithelial models, there was less transmigration of Detroit 562 nasopharyngeal epithelial cells by the mutants compared to WT. Cellular reorganisation of primary human airway epithelium varied considerably between strains. Compared to WT, infection of Detroit 562 epithelial cells by the Δ*fhs/piaA* strain, but not the Δ*proABC/piaA* strain was less pro-inflammatory, induced less caspase 8 production, and were associated with increased pneumococcal hydrogen peroxide and reduced pneumolysin secretion.

These findings suggest that the observed differences in microinvasion and the epithelial response were driven by the differential expression of multiple bacterial virulence and metabolic pathways, rather than single genes or pathways of genes. These data highlight the complex impact of single gene mutations on bacterial virulence and suggest that the virulence determinants of pneumococcal epithelial colonisation, microinvasion and innate immunity are not necessarily directly linked to disease.

Author Summary

Streptococcus pneumoniae (the pneumococcus) commonly colonises the back of the human nose, and is a leading cause of pneumonia, meningitis, and sepsis. During colonisation, the pneumococcus adheres to the cells in the nose, invades these cells (so-called microinvasion), and activates them.

Colonisation is a pre-requisite for disease, however, since disease is largely a dead end for *S. pneumoniae*, it remains unclear whether these processes are directly linked to disease progression. We have previously shown that if we introduce gene mutations into *S. pneumoniae* that affect key metabolic pathways, these bacteria retain their ability to colonize human and animal models without causing disease. We now show that these mutants retain their ability to microinvade epithelial cells in human and mouse models, and some may still cause inflammation, but are less able to pass through the epithelial barrier. However, although the attenuation of disease may be explained by the broad-ranging impact of these mutations on pneumococcal virulence, oxidative stress, and metabolism, they are not driven by a single determinant. Our findings suggest that pneumococcal microinvasion and immune activation are not necessarily pre-cursors to disease progression. This supports the idea that *S. pneumoniae* adapts and evolves to promote colonisation and ultimately transmission rather than cause disease.

Keywords

Biosynthesis genes, host-pathogen interactions, Innate immunity, *Streptococcus pneumoniae*, airway epithelium, colonisation, disease

Graphical Abstract

S. pneumoniae colonisation is characterised by mucus association, epithelial adherence, microcolony formation and microinvasion – where the pneumococcus invades the epithelial barrier without causing disease. Although mutations in *S. pneumoniae* biosynthesis genes (Δ*proABC* and Δ*fhs*) attenuate disease in a murine model, they do not attenuate microinvasion in either experimental human pneumococcal challenge (EHPC), *ex vivo* or *in vitro* epithelial cells. Transmigration of the epithelial barrier is attenuated. These mutations show strain-dependent effects on both the epithelial and bacterial responses to infection. Factors such as epithelial cellular reorganisation, inflammation and caspase 8 activity alongside pneumococcal metabolic adaptation, virulence factor expression and response to stress are important components of these processes.

INTRODUCTION

Streptococcus pneumoniae is a common commensal of the URT, yet translocation of the pneumococcus to the lungs, blood or the brain leads to life-threatening disease [1]. Among children under five, *S. pneumoniae* is the leading cause of pneumonia-related deaths globally [2].

We have previously shown that *S. pneumoniae* colonisation is characterised by epithelial surface microcolony formation and invasion, termed microinvasion [3]. Pneumococcal colonization elicits an innate immune response that may facilitate clearance while also promoting bacterial transmission [3, 4]. Beyond the capsule, numerous virulence factors have evolved to optimise colonization and transmission, rather to cause invasive disease. We therefore hypothesize that epithelial microinvasion and the innate immune response to colonization are not necessarily linked to disease causation.

To test this, we have used two *S. pneumoniae* serotype 6B biosynthesis gene mutants (Δ*proABC* and Δ*fhs*), which were designed to induce protective immunity through nasopharyngeal colonization without causing disease [5]. The *proABC* operon encodes enzymes for proline biosynthesis, while *fhs* encodes a tetrahydrofolate reductase involved in one-carbon metabolism, both essential for pneumococcal growth and virulence [6-8]. In murine models, these mutants colonize the nasopharynx but fail to cause invasive disease [5, 8]. In EHPC, Δ*proABC* and Δ*fhs* mutants carrying an additional *piaA* deletion (disrupting a key iron uptake transporter, introduced to prevent reversion) retained the ability to colonise and elicit IgG-mediated immunity [9, 10], [10]. These isogenic mutants thus provide a controlled system to investigate epithelial microinvasion and innate immune activation independently of capsular serotype.

106 Here, we show that although the Δ*proABC/piaA* and Δ*fhs/piaA* mutations attenuate disease through
107 broad-ranging impacts on pneumococcal virulence, oxidative stress, and metabolism, and reduced
108 epithelial transmigration, they retained the capacity to colonize and invade epithelial cells. The Δ*fhs*
109 but not the Δ*proABC* mutant was less pro-inflammatory. Hence pneumococcal microinvasion and
110 immune activation are not necessarily pre-cursors to disease progression, highlighting the complex
111 impact of biosynthesis gene mutations on pneumococcal virulence, with differential effects on
112 epithelial colonisation and disease.

113

114 **RESULTS**

115

116 **Deletion of the *proABC* and *fhs* genes have broad-ranging differential effects on the *S.***
117 ***pneumoniae* virulence gene expression and metabolic gene pathways when under stress**

118 We have previously shown that Δfhs and ΔproABC showed considerable derangement in global
119 gene transcription when cultured in human serum compared to growth under optimal nutrient
120 conditions [8]. Metabolic analysis suggested that in sera, Δ*fhs* had an impaired stringent response,
121 and both mutants were under increased oxidative stress and had altered lipid profiles [8]. The
122 Δ*proABC* mutation resulted in the accumulation of glycolytic pathway and peptidoglycan synthesis
123 intermediates. To further understand links between disease attenuation, epithelial colonisation and
124 the innate immune response, we extended the transcriptomic analysis of the mutants' responses to
125 serum stress [8]. This revealed upregulation of virulence factors such as *ply*, *nanA*, *psaA,* those
126 regulating oxidative stress like *SpxB*, *lctO* and *adhE*, and genes involved in purine and carbohydrate
127 metabolism (Supplemental Information Table 1). Phosphotransferase systems, amino nucleotide
128 sugar, fructose and mannose and metabolic pathways were the most significantly enriched pathways
129 in the Δ*proABC* mutant (Table 1). In contrast, competence, purine, pyruvate, metabolic pathways,
130 amino nucleotide sugar pathways and secondary metabolites were the most significantly enriched
131 pathways in the Δ*fhs* mutant under stress (Table 1).

132

133 **Table 1. Differentially expressed pathways from single isogenic mutants in human serum**
134 **compared to WT.**

135

Pathway	GeneRatio	P-adjust	qvalue
Δ*fhs* vs. WT			
Fatty acid metabolism/biosynthesis	10/57	1.08E-09	6.49E-10
Biosynthesis of secondary metabolites	26/57	2.09E-04	1.26E-04
Purine metabolism	10/57	1.34E-03	8.06E-04
Quorum sensing	11/57	3.20E-03	1.92E-03
Pantothenate and CoA biosynthesis	5/57	3.59E-03	2.16E-03
beta-Lactam resistance	5/57	7.59E-03	4.57E-03
Propanoate metabolism	4/57	1.51E-02	9.09E-03
2-Oxocarboxylic acid metabolism	4/57	1.51E-02	9.09E-03
Metabolic pathways	40/57	1.94E-02	1.16E-02
Amino sugar and nucleotide sugar metabolism	7/57	4.22E-02	2.54E-02
Pyruvate metabolism	5/57	4.31E-02	2.59E-02
Δ*proABC* vs. WT			
Fatty acid metabolism/biosynthesis	10/71	1.17E-08	8.94E-09
Galactose metabolism	12/71	1.25E-04	2.47E-08
Phosphotransferase system (PTS)	13/71	2.54E-03	1.93E-03
Amino sugar and nucleotide sugar metabolism	9/71	2.89E-02	2.20E-02

136

137 **Table 1. Differentially expressed pathways from single isogenic mutants in human**
138 **serum compared to WT.** 55 genes were selected within competence pathways, amino acid

139 metabolism, virulence factors, oxidative stress pathways and other known genes important
140 for colonisation, for assessment of changes in gene expression following serum stress. *q-*
141 *value* measures the proportion of false positives incurred (the false discovery rate) when
142 that particular test is significant.

143

144 ***S. pneumoniae* 6B disease-attenuated mutants colonise and microinvade nasal epithelium in**
145 **EHPC**

146 We investigated whether the Δ*proABC/piaA* or Δ*fhs/piaA* mutations affected epithelial association
147 and microinvasion (Fig 1A) using nasal curette samples from EHPC of healthy volunteers [11].
148 Visualisation of mucosal cells by confocal microscopy showed colonisation by the WT and mutant
149 pneumococcal strains at day 6 post challenge (Fig 1B): 4/11 volunteers challenged with the WT,
150 5/11 volunteers with the Δ*proABC/piaA, and* 4/5 volunteers with the Δ*fhs/piaA*. Microinvasion
151 (intracellular bacteria) was seen in 2/11 volunteers with the WT, 5/11 volunteers with the
152 Δ*proABC/piaA,* and 3/5 volunteers with the Δ*fhs/piaA* (Fig 1C). Together, these data show that
153 compared to WT, there was no attenuation of colonisation or microinvasion with either the
154 Δ*proABC/piaA* or Δ*fhs/piaA* strains in EHPC.

155

156 **Colonisation and microinvasion of human airway epithelium by the disease-attenuated**
157 **mutants is associated with cellular reorganisation and preservation of barrier function**

158 To explore whether disease-attenuation influences epithelial cellular organisation, we infected
159 normal human bronchial epithelial airway (NHBE-A) cells with these pneumococcal strains. We
160 observed epithelial association and microinvasion with all three strains (Fig 2A, top). TEM
161 demonstrated that the intracellular bacteria for all three strains were likely enclosed within vacuoles
162 (Fig 2A, bottom). WT and mutant strains co-localised with Junctional Adhesion Molecule A (JAM-A,
163 Fig 2B, arrow), with no change in JAM-A expression. Quantification by image analysis demonstrated
164 differential effects on the expression of other junctional proteins with increased intensity of Zonula
165 Occludens 1 (ZO-1) at the junctional membrane after infection with WT (Fig 2C), and increased

166 intensity of β catenin staining infected with either Δ*proABC/piaA or* Δ*fhs/piaA*, compared to cells
167 exposed to these strains but not infected (Fig 2D), suggesting cellular reorganisation following
168 pneumococcal exposure.

169

170 NHBE cells cultured at an air-liquid interface differentiate into a pseudostratified columnar ciliated
171 epithelium, consisting of goblet, Clara, basal and ciliated cells (Fig 3A). Following infection, strains
172 were observed amongst cilia (acetylated tubulin positive cells, Fig 3B, Supplemental Information Fig
173 1) and the Δ*proABC/piaA* co-localised with mucus (mucin5ac positive, Fig 3C, arrows). Infection with
174 WT and Δ*proABC/piaA* but not Δ*fhs/piaA* resulted in an increased abundance of secreted mucus
175 globules compared to uninfected cells (Fig 3A). This appeared due to secretion of preformed mucus
176 rather than de-novo production, as expression of Mucin5AC was unaffected (Fig 3C). Infection with
177 the Δ*proABC/piaA* strain increased expression of acetylated tubulin within pneumococcal-associated
178 cells (Fig 3B), known to be associated with increased microtubule conformation and elasticity [12,
179 13]. In contrast, only infection with Δ*fhs/piaA* caused increased expression of uteroglobin, a
180 multifunctional epithelial secreted protein with anti-inflammatory and anti-chemotactic properties,
181 and a marker for non-ciliated Clara cells (Fig 3D).

182

183 **Δ*fhs/piaA* but not the Δ*proABC/piaA* mutations attenuate the pro-inflammatory epithelial**
184 **innate response to pneumococcal colonisation and microinvasion**

185 We have shown that Detroit 562 epithelial nasopharyngeal cells are a good model for responses to
186 *S. pneumoniae* [3]. Indeed, infection of Detroit 562 cells showed that WT, Δ*proABC/piaA* and
187 Δ*fhs/piaA* strains formed colonies on the epithelial surface (Fig 4A), with limited differences between
188 these strains (Fig 4B, top left). Microinvasion of Detroit 562 cells was observed with all strains (Fig
189 4B, top right) and showed no differences in intracellular viability (Fig 4B, bottom left) or replication
190 (Supplemental Information Fig 2A-F). In line with attenuation of disease, the Δ*proABC/piaA* and
191 Δ*fhs/piaA* were impaired in their ability to transmigrate across the epithelium (Fig 4B, bottom right).
192 Importantly, the single Δp*iaA* mutation in the *S. pneumoniae* serotype 6B did not affect epithelial

193 association, microinvasion and transmigration, linking the differences seen to the Δ*fhs* and Δ*proABC*
194 mutations (Fig 4B). Epithelial β catenin expression was also affected following incubation with the
195 Δ*proABC/piaA* and Δ*fhs/piaA* strains, compared to the WT in pneumococcal-associated and non-
196 associated cells. (Fig 4C).
197

198 We further assessed links between colonisation, microinvasion and epithelial cell innate immunity
199 using RNAseq. Compared to non-infected cells (Fig 5A), all strains upregulated 78 core epithelial
200 genes related to cytokine signalling in immune system, NLR signalling and GPCR ligand binding.
201 193 genes were upregulated in response to WT and Δ*proABC/piaA*, characterised by Rhodopsin-
202 like receptors, GPCR ligand binding, cytokine signalling in Immune system, signalling by interleukins
203 and Toll Receptor cascades. Infection with Δ*fhs/piaA* resulted in a markedly different transcriptomic
204 profile with modest upregulation of 254 genes, characterised by antigen processing, proteasomal
205 pathways, GTP hydrolysis, and intracellular stress responses (Fig 5A). Overall, the epithelial genes
206 that were most upregulated following infection with WT or Δ*proABC/piaA* were similar and contrasted
207 to the reduced gene expression profile in response to Δ*fhs/piaA* despite high levels of cell invasion
208 (Fig 5B). Transcription factors, cellular kinases and cytokines (Fig 5C, 5D) predicted to regulate the
209 differentially expressed genes showed the greatest difference in profile following infection with
210 Δ*fhs/piaA* compared to infection with 6B WT and Δ*proABC/piaA*. Δ*fhs/piaA* was associated with
211 diminished NFκB and MAPK activation and instead induced a more intrinsic and epithelial repair
212 response that included TBK1, Raf1, JAK1 kinases and IL-1 and IL-33 cytokine signalling. These data
213 therefore suggest that attenuation of disease-causing potential is not dependent on a reduction in
214 the epithelial innate immune response to colonisation.
215

216 **Enhanced epithelial caspase 8 activity following infection with wild-type and Δ*proABC/piaA***
217 **strains**

218 To further explore the link between disease attenuation and the epithelial innate immune response
219 to colonisation, we assessed differential caspase activation. The NLRP3 inflammasome drives
220 programmed epithelial cell death via caspase 1, caspase 3/7 and caspase 8 activity [14].

221

222 Compared to non-infected cells, all strains increased epithelial caspase activity 6-hour post infection,
223 although this was only significant following infection with Δ*proABC/piaA* (Fig 6A, dark grey bars).
224 Incubating infected cell cultures with either a caspase 1 inhibitor (YVAD-CHO) or caspase 3/7
225 inhibitor (Z-VAD-FMK), showed that increased caspase activation following infection with WT and
226 Δ*fhs/piaA* was not due to caspase 1 activity (Fig 6B)Compared to non-infected cells, caspase 3/7
227 accounted for 3% and 15% of the caspase activity induced following infection with WT and Δ*fhs/piaA*
228 respectively (Fig 6A). In contrast, Δ*proABC/piaA* strain did not induce caspase 3/7 activity. Caspase
229 8 activation was significantly increased following epithelial infection with 6B WT and Δ*proABC/piaA*
230 strain (Fig 6C).

231

232 ***fhs* gene mutation is associated with increased pneumococcal hydrogen peroxide secretion**
233 **and decreased pneumolysin activity**

234 *S. pneumoniae* SpxB and LctO generate hydrogen peroxide (H_2O_2) which suppresses ENaC-α
235 transcription and inhibits the Na+–K+ pump, an intracellular signal to increase mitochondrial ROS
236 production [15, 16]. We postulated that differences in cellular reorganisation, the innate inflammatory
237 response and caspase 8 activation seen between Δ*proABC/piaA* and Δ*fhs/piaA* mutants could be
238 explained by differential expression of pneumococcal H_2O_2. After three and six hours, we detected
239 significantly higher levels of H_2O_2 in Δ*fhs/piaA* cultures compared to 6B WT and Δ*proABC/piaA*
240 strains (Fig 7A). Furthermore, this was maintained during epithelial cell contact (Fig. 7B).

241

242 Pneumolysin can both activate and suppress the host innate immune response and mediates the
243 haemolytic activity characteristic of the pneumococcus [17-19]. H_2O_2 increases the release of

244 pneumolysin but paradoxically also negatively impairs its haemolytic activity [20]. In line with this
245 paradoxical effect the higher production of H_2O_2 by the Δ*fhs/piaA* strain, was associated with
246 increased *ply* gene expression but reduced red blood cell lysis compared to 6B WT and
247 Δ*proABC/PiaA* (Fig. 7C).

248

249

250 **DISCUSSION**

251 We show that when using isogenic serotype 6B biosynthesis pathway mutant strains, attenuated for
252 systemic disease but not for carriage, epithelial microinvasion is preserved [5, 8, 21]. Epithelial
253 barrier transmigration was significantly less with the isogenic strains with the Δ*fhs/piaA* and
254 Δ*proABC/piaA* mutations compared to WT *S. pneumoniae* 6B. Importantly, while epithelial
255 microinvasion, cellular reorganization, the innate epithelial immune response, and the propensity to
256 cause invasive disease following pneumococcal colonisation are all strain-dependent, no single
257 determinant explained these differences.

258

259 In our primary epithelial cell infection model [22], consisting of Clara cells (involved in secretory,
260 xenobiotic metabolic, and progenitor cell functions), goblet cells (mucus production), ciliated cells
261 (small particle transport), infection with WT and mutant strains resulted in epithelial cellular re-
262 organisation involving β catenin, acetylated tubulin and uteroglobin. However, strain differences
263 seen on the impact on junctional or cytoskeletal protein organisation or mucus production did not
264 explain the disease attenuation seen with Δ*fhs/piaA* and Δ*proABC/piaA*.

265

266 Epithelial infection with WT and Δ*proABC/piaA* induced innate inflammatory pathway gene
267 expression [3], including cytokine/chemokines, interleukins, Toll Like Receptor and NFκB signalling,
268 alongside apoptotic transcripts such as FOXO3 and TP53. Notably, some epithelial genes were

269 upregulated exclusively during WT infection, which could be related to its greater disease-causing
270 potential. These were involved in RNA degradation, O-linked glycosylation, wnt signalling, DNA
271 sensing, RIG-I pathways all of which play a role in the immune response and signal transduction. In
272 contrast, the Δ*fhs/piaA* strain activated a distinct pro-survival and adaptation profile, upregulating
273 genes such as JUN, SMARCA4, NFAT5, KLF6 and TCF4 which are involved in homeostatic
274 signalling and chromatin remodelling [23, 24], and suggesting a more tolerant epithelial response to
275 this strain. Ultimately, these capsule-independent differences in pneumococcal-epithelial
276 interactions may shape the differences seen in adaptive immune response identified using EHPC to
277 colonisation with the WT, Δ*proABC/piaA* or Δ*fhs/piaA* strains [11, 25].

278

279 Importantly, while all strains adhered and microinvade the epithelium, WT serotype 6B infection led
280 to pneumococcal transmigration, a more pro-inflammatory innate immune transcriptomic profile and
281 increased caspase 8 activity, indicative of a robust cellular response to *S. pneumoniae*, with
282 Δ*proABC/piaA* and Δ*fhs/piaA* exhibiting attenuation of these responses. This suggests that
283 pneumococcal sensing by the epithelium is affected by disruption of *S. pneumoniae* metabolism [18,
284 26]. Pneumolysin is a key driver of epithelial inflammatory responses and increased acetylated
285 tubulin and microtubule stabilisation [13] [3]. Under stress conditions, the Δ*proABC* and Δ*fhs*
286 mutations upregulated multiple metabolic pathways, presumably as a compensatory mechanism,
287 and also genes encoding several pneumococcal virulence factor genes (Graphical Abstract
288 Summary) including pneumolysin and H_2O_2. Based on these findings, we propose that differential
289 expression of pneumolysin, and H_2O_2 by the WT and mutant strains may contribute to the distinct
290 patterns of epithelial responses that we observed, with the potential to influence both bacterial
291 clearance and transmission [1]. Whether the distinct epithelial innate immune response to Δ*fhs/piaA*
292 infection is due to diminished NFκB and MAPK activation (potentially linked to extracellular receptor
293 engagement), reduced caspase 8 activity mediated by enhanced pneumococcal H_2O_2 release,
294 decreased pneumolysin activity, or a compensatory metabolic response to the stress, remains to be
295 determined. As seen in 'professional' intracellular bacterial species such as *Listeria* and *Salmonella*,
296 the host response to microinvasion might also promote pneumococcal transmission [27, 28].

297 Whether the less pro-inflammatory Δ*fhs/piaA* is less transmissible than the more inflammatory WT
298 is unknown, which could be explored using the EHPC model [29].

299

300 In conclusion, these data further support our proposed paradigm that epithelial microinvasion by *S.*
301 *pneumoniae* is frequent and does not necessarily lead to disease. Microinvasion may aid
302 transmission through immune evasion and localised inflammation and, transmigration across the
303 epithelium may represent the first step towards transition to invasive disease. Our findings also
304 highlight the broad-ranging effects of single gene mutations in pneumococcal biosynthesis
305 pathways, which may explain the complexity of differences between seemingly closely related
306 strains. The interplay between *S. pneumoniae* and the host epithelium is modulated by key mediators
307 such as hydrogen peroxide and pneumolysin, which can have both enhancing and inhibitory effects
308 on epithelial immune responses depending on the infection context. However, strain differences in
309 subsequent epithelial cell microinvasion, cellular reorganisation and inflammatory responses appear
310 driven by the differential expression of multiple bacterial virulence and metabolic pathways, rather
311 than any single determinant.

312

313 **METHODS AND PROTOCOLS**

314

315 **Bacteria**

316 The *Streptococcus pneumoniae* serotype 6B (strain BHN 418 [30]) was a kind gift from Prof. Birgitta
317 Henriques Normark (Karolinska Institute). Δ*proABC/piaA* and Δ*fhs/piaA* mutant strains were
318 generated using overlap extension PCR as described by Ramos-Sevillano *et al* [5]. Aliquot stocks
319 frozen at 0.3 $O.D._{600nm}$ were defrosted, centrifuged at 8000g for eight minutes and resuspended in
320 1% Foetal Bovine Serum (FBS, Gibco) in MEM media (Gibco) for infections. Starting inoculums were
321 not significantly different across strains for all assays.

322

323 **Bacterial RNA-seq sample collection, sequencing and reads**

324 Pneumococcal strains were grown in THY to mid-log phase and pellets resuspended in THY and
325 undiluted human serum for 60mins. The culture was centrifuged and stored in RNA Protect at -70°C
326 before extracting total RNA [8]. Total RNA from each library was ribo-depleted and sent for Illumina
327 Next Seq Sequencing Pathogen Genomics Unit, UCL, as detailed in Supplemental Information.

328

329 **Differential gene expression analyses**

330 The generated count matrix was imported into R-studio (R v3.4.2) and normalization of counts and
331 differential gene expression analysis was performed by DESeq2 [31]. DESeq2 normalized libraries
332 were regularized log transformed for visualizing heatmaps and clustering. Differential gene
333 expression was performed on raw counts. Fold change shrinkage was implemented with the apeglm
334 package within DESeq2. Genes with a log2 fold change > 1.5 and false discovery rate (FDR) of <
335 0.05 were categorized as differentially expressed. KEGG pathway enrichment and module analysis
336 were performed on differentially regulated genes using over representation analysis (ORA)
337 implemented by clusterProfiler [32].

338

339 **Experimental Human Pneumococcal Carriage Model (EHPC)**

340 A full explanation of experimental design and selection criteria has been previously described [3]
341 and detailed in Supplemental Information.

342

343 **Normal Human Epithelial Cells**

344 Normal Human Bronchial/Tracheal Epithelial Cells (NHBE-A, ATCC® PCS-300-010™) were plated
345 at 6x10^{3} cells/cm^{2} on a layer of sub-lethally γ-irradiated (60 Gy) mouse embryonic fibroblasts 3T3-
346 J2 cells (kind donation from Howard Green, Harvard Medical School, Boston [33]) with keratinocyte
347 culture medium cFAD (3:1 DMEM (Gibco) to Ham F-12 Nut Mix (Gibco), 10% FBS (HyClone, Sigma),
348 1% Penicillin-Streptomycin (100X, Sigma), 0.4 µg/mL Hydrocortisone (Calbiochem, USA), 5 µg/ml
349 Insulin (various), 10-10 Cholera Toxin (Sigma) and 2x10-9 Triodothyronine (Sigma)). Epithelial cells

350 were stimulated with 10 ng/mL human epidermal growth factor (hEGF, PeproTech, USA) on days 3
351 and 5. Cultures were grown at 37°C 6% CO_2. For NHBE-A differentiation in Air Liquid Interface
352 culture, cells were plated at $6x10^4/cm^2$ on 1µm pore PET cell culture inserts (Greiner). All chambers
353 were supplemented with cFAD medium. After 48 hours, medium was removed from the top chamber.
354 Lower chamber media was replaced with PneumaCult™ differentiation Medium (Stemcell
355 Technologies) every 2 days for 3 weeks. Antibiotics were removed from media and cells were
356 washed 24 hours before infection experiments.

357

358 **Human Epithelial Cell Lines**

359 Human pharyngeal carcinoma Detroit 562 epithelial cells (ATCC_CCL-138) were grown in 10% FCS
360 in alpha MEM media (Gibco). For each set of experiments, cells were used within 5 passages. Cells
361 consistently tested PCR negative for mycoplasma (Cambridge Biosciences).

362

363 **Pneumococcal-epithelial cell co-culture**

364 For association and internalisation assays, confluent monolayers of Detroit 562 cells cultured on 12
365 well plates (Corning), were infected(1 cell to 10 pneumococci) for three hours in 1% FCS MEM or
366 six hours for HNBE-A cells in 1% Pneumocult media without supplements [3]. Cells washed three
367 times in $HBSS^{+/+}$ before incubation in 1% saponin for 10 minutes at 37°C. Bacterial dilutions were
368 plated on horse blood agar for 16 hours and colony forming units counted. For internalisation
369 quantification, 200µg/ml gentamicin was added one hour before incubation with saponin.

370

371 For transmigration assays, confluent monolayers of Detroit 562 cells cultured on 3µm pore, PET
372 Transwell Inserts (ThermoFisher) [3] were infected for three hours. 50µl of basal media was
373 repeatedly removed to measure pneumococcal load by counting CFU/well.

374

375 **Confocal Microscopy**

376 Epithelial monolayers on transwell membranes were infected then fixed in 4% PFA (Pierce, Methanol
377 Free) as previously described and detailed in Supplemental Information [3]. Cells were processed

378 for image analysis using an inverted Zeiss LSM (either 700 or 880). Z stacks were recorded at 1µm
379 intervals at either 40x oil or 63x oil objectives. Automated image analysis was carried out using
380 Cellprofiler [34].

381

382 **Electron Microscopy**

383 Preparation of Detroit 562 cells and NHBE-A cells was performed as previously described and details
384 can be found in Supplemental Information [3].

385

386 **Pneumolysin activity**

387 Adapted from Kirkham *et al* [35]. Final concentration of 2% horse blood (EO Labs) solution was
388 prepared in phenol free alpha MEM (Life Technologies) and added to a 96 U-bottom plate (Corning).
389 $2.5x10^6$ bacteria were added to 96 well. Saponin was used as a positive control for lysis. Solutions
390 were incubated for 30 minutes at 37°C before centrifugation at 1000g for one minute. Solution was
391 transferred into a new 96 well plate and absorbance recorded at 540nm on a plate reader.

392

393 **Hydrogen Peroxide Assay**

394 Detroit 562 cells were cultured in white 96 well plates (Corning). Cells were incubated with H_2O_2
395 substrate and infected for up to six hours according to manufacturers' instructions (ROS-Glo^{TM} H_2O_2
396 Assay, Promega). Luminescence was read using a GloMax -Multi Detection System plate reader
397 (Promega).

398

399 **Caspase assay**

400 Detroit 562 cells were cultured in white 96 well plates (Corning). Cells were infected for up to six
401 hours. Primary cell supernatant was transferred to a white 96 well plate. Samples were incubated
402 with Caspase-Glo® 1 Reagent, Caspase-Glo® 1 YVAD-CHO Reagent, Caspase-Glo® Z-VAD-FMK
403 Reagent or Caspase-Glo® 8 Reagent, for one hour and according to manufacturers' instructions
404 (Promega). Luminescence was read using a GloMax-Multi Detection System plate reader
405 (Promega).

406

407 **RNA samples and sequencing (RNA-Seq)**

408 Confluent monolayers of Detroit 562 epithelial cells were infected for four hours before collection in
409 RNALater. RNA was extracted using a Qiagen RNAEasy micro kit and treated for DNA removal
410 using a Qiagen Turbo DNA-free kit. RNA quality was assessed and quantified using a BioAnalyser
411 (Agilent 2100). Samples were sequenced using Illumina Nextseq 500/550 High Output 75 cycle kit
412 giving 15-20 million 41bp paired-end reads per sample (Pathogens Genomic Unit, UCL).

413

414 **Statistics**

415 Conditions within each experiment were performed in duplicate or triplicate, and each experiment
416 was performed independently more than three times, unless stated otherwise. Error bars represent
417 SEM, unless stated otherwise. GraphPad Prism Version 7 was used for parametric (t-tests or
418 ANOVA) or non-parametric (Mann-Whitney or Kruskal-Wallis tests) analysis, which was based on
419 the Shapiro-Wilk normality test. Ad hoc tests were performed using Tukey's (parametric data) or
420 Dunn's (non-parametric data) multiple comparisons test. P values <0.05 were considered significant.

421

422 **Data and code availability**

423 Source data are provided as a Source Data file. RNAseq data from the Detroit 562 cell infections is
424 publicly accessible through Zenodo with Accession (DOI:10.5281/zenodo.7997789).

425

426 **ACKNOWLEDGEMENTS**

427 This study was funded by CMW from a Postdoctoral Innovation Award from UCL, a Pump-Priming
428 Award and Enhancement Award from the Human Infection Challenge Network for Vaccine
429 Development (HIC-VAC (funded by the GCRF Networks in Vaccines Research and Development)
430 which is co-funded by the MRC and BBSRC). This UK funded award is part of the EDCTP2
431 programme supported by the European Union. CMW and RSH are supported by the Medical

432 Research Council (grant MR/T016329/1). The authors would like to thank Prof. Peter Hermans
433 (Radboud University Medical Centre) for donating the 6B pneumococcal strain originally from Prof.
434 Birgitta Henriques-Normark (Karolinska Institute) and obtained directly from DF at LSTM. EHPC
435 sample collection was supported by the Medical Research Council (grant MR/M011569/1), Bill and
436 Melinda Gates Foundation (grant OPP1117728) awarded to DF and the National Institute for Health
437 Research (NIHR) Local Comprehensive Research Network. The authors also wish to thank the
438 EHPC Clinical Team at LSTM and all the volunteers. Confocal imaging facilities at LSTM were
439 funded by a Wellcome Trust Multi-User Equipment Grant (104936/Z/14/Z). Electron microscopy
440 processing and image capture was performed by Dr. Elizabeth Slavik-Smith in the Biosciences EM
441 facility at UCL. MC is supported by a Springboard to Independence grant (AirwayStasis) from the
442 French Government's Investissement d'Avenir program, the Laboratoire d'Excellence ''Integrative
443 Biology of Emerging Infectious Diseases" (ANR-10-LABX-62-IBEID) and the Chromatin and infection
444 unit headed by Melanie A. Hamon. RNA-Seq library preparation was undertaken at UCL through the
445 UCL/UCLH Biomedical Research Centre and MRC funded Pathogen Genomics Unit (PGU,
446 G0900950). All RNAseq data processing was completed by the PGU. MN is supported by the
447 Wellcome Trust and by NIHR Biomedical Research Centre Funding to University College Hospitals
448 NHS Foundation Trust and University College London. RR is supported by Marie Skłodowska-Curie
449 Individual Fellowships 896014. PB is supported by the European Research Council (ERC-Stg No.
450 639429), the Rosetrees Trust (M362-F1; M553), the CF Trust (SRC006;SRC020), the London
451 Advanced Therapies - Research England (C2N-AT.006), the MRC Confidence in Concept scheme
452 (Award: MC_PC_17180), the Innovate UK (Smart grant n.10005465), the Duchenne Parent Project
453 (DPP) and the NIHR GOSH BRC. MW is supported by a 223065 Wellcome Investigator Award to
454 Clare Jolly, UCL. ERS and JSB are supported by MRC grant R/N02687X/1 and Wellcome grant
455 221803/Z/20/Z. JSB, MN, and RSH acknowledge funding from the Department of Health's National
456 Institute of Health and Care Research Biomedical Research Centre funding to UCL and UCLH. RSH
457 is a NIHR Senior Investigator.
458

AUTHOR CONTRIBUTIONS: CMW conceived, funded, designed and conducted the study, performed the experiments, acquired samples and processed data, and wrote the first draft of the manuscript. GP analysed and interpreted the RNAseq data. MB analysed and interpreted the bacterial transcriptomic data. RR cultured and differentiated primary epithelial cells. ERS generated the 6B mutant strains and bacterial transcriptomic data. JR collected and processed EHPC samples. JAGA processed the RNA-Seq data. MW ran the image analysis. MC provided technical advice. PB and CJ provided investigator support. MN provided RNA-Seq analysis support. DF provided investigator support and EHPC clinical samples. JSB generated the 6B mutant strains, interpreted the data and revised the manuscript. RSH provided investigator support, designed and interpreted the data, revised the manuscript. All authors commented on and approved the manuscript.

COMPETING INTERESTS: The authors declare no competing interests.

REFERENCES

1. Weiser JN, Ferreira DM, Paton JC. Streptococcus pneumoniae: transmission, colonization and invasion. Nat Rev Microbiol **2018**; 16:355-67.
2. O'Brien KL, Wolfson LJ, Watt JP, et al. Burden of disease caused by Streptococcus pneumoniae in children younger than 5 years: global estimates. Lancet **2009**; 374:893-902.
3. Weight CM, Venturini C, Pojar S, et al. Microinvasion by Streptococcus pneumoniae induces epithelial innate immunity during colonisation at the human mucosal surface. Nat Commun **2019**; 10:3060.
4. Zafar MA, Hamaguchi S, Zangari T, Cammer M, Weiser JN. Capsule Type and Amount Affect Shedding and Transmission of Streptococcus pneumoniae. MBio **2017**; 8:e00989-17.
5. Ramos-Sevillano E, Ercoli G, Felgner P, et al. Preclinical Development of Virulence-attenuated Streptococcus pneumoniae Strains Able to Enhance Protective Immunity against Pneumococcal Infection. Am J Respir Crit Care Med **2021**; 203:1037-41.
6. Brill J, Hoffmann T, Bleisteiner M, Bremer E. Osmotically controlled synthesis of the compatible solute proline is critical for cellular defense of Bacillus subtilis against high osmolarity. J Bacteriol **2011**; 193:5335-46.
7. Crowley PJ, Gutierrez JA, Hillman JD, Bleiweis AS. Genetic and physiologic analysis of a formyl-tetrahydrofolate synthetase mutant of Streptococcus mutans. J Bacteriol **1997**; 179:1563-72.
8. Ramos-Sevillano E, Ercoli G, Betts M, et al. Essential role of proline synthesis and the one-carbon metabolism pathways for systemic virulence of Streptococcus pneumoniae. mBio **2024**; 15:e0175824.
9. Brown JS, Gilliland SM, Holden DW. A Streptococcus pneumoniae pathogenicity island encoding an ABC transporter involved in iron uptake and virulence. Mol Microbiol **2001**; 40:572-85.
10. Hill H, Mitsi E, Nikolaou E, et al. A Randomized Controlled Clinical Trial of Nasal Immunization with Live Virulence Attenuated Streptococcus pneumoniae Strains Using Human Infection Challenge. Am J Respir Crit Care Med **2023**; 208:868-78.

496 11. Ferreira DM, Neill DR, Bangert M, et al. Controlled human infection and rechallenge with Streptococcus
497 pneumoniae reveals the protective efficacy of carriage in healthy adults. Am J Respir Crit Care Med **2013**;
498 187:855-64.
499 12. Eshun-Wilson L, Zhang R, Portran D, et al. Effects of alpha-tubulin acetylation on microtubule structure
500 and stability. Proc Natl Acad Sci U S A **2019**; 116:10366-71.
501 13. Iliev AI, Djannatian JR, Opazo F, et al. Rapid microtubule bundling and stabilization by the Streptococcus
502 pneumoniae neurotoxin pneumolysin in a cholesterol-dependent, non-lytic and Src-kinase dependent
503 manner inhibits intracellular trafficking. Mol Microbiol **2009**; 71:461-77.
504 14. Surabhi S, Jachmann LH, Shumba P, Burchhardt G, Hammerschmidt S, Siemens N. Hydrogen Peroxide Is
505 Crucial for NLRP3 Inflammasome-Mediated IL-1beta Production and Cell Death in Pneumococcal Infections
506 of Bronchial Epithelial Cells. J Innate Immun **2022**; 14:192-206.
507 15. Erttmann SF, Gekara NO. Hydrogen peroxide release by bacteria suppresses inflammasome-dependent
508 innate immunity. Nat Commun **2019**; 10:3493.
509 16. Alibayov B, Scasny A, Khan F, et al. Oxidative Reactions Catalyzed by Hydrogen Peroxide Produced by
510 Streptococcus pneumoniae and Other Streptococci Cause the Release and Degradation of Heme from
511 Hemoglobin. Infect Immun **2022**; 90:e0047122.
512 17. Zafar MA, Wang Y, Hamaguchi S, Weiser JN. Host-to-Host Transmission of Streptococcus pneumoniae Is
513 Driven by Its Inflammatory Toxin, Pneumolysin. Cell Host Microbe **2017**; 21:73-83.
514 18. Periselneris J, Turner CT, Ercoli G, et al. Pneumolysin suppresses the initial macrophage pro-inflammatory
515 response to Streptococcus pneumoniae. Immunology **2022**; 167:413-27.
516 19. Terra VS, Plumptre CD, Wall EC, Brown JS, Wren BW. Construction of a pneumolysin deficient mutant in
517 streptococcus pneumoniae serotype 1 strain 519/43 and phenotypic characterisation. Microb Pathog **2020**;
518 141:103999.
519 20. Bazant J, Ott B, Hudel M, Hain T, Lucas R, Mraheil MA. Impact of Endogenous Pneumococcal Hydrogen
520 Peroxide on the Activity and Release of Pneumolysin. Toxins (Basel) **2023**; 15.
521 21. Ramos-Sevillano E, Ercoli G, Guerra-Assuncao JA, et al. Protective Effect of Nasal Colonisation with
522 cps/piaA and cps/proABCStreptococcus pneumoniae Strains against Recolonisation and Invasive Infection.
523 Vaccines (Basel) **2021**; 9.
524 22. Travaglini KJ, Nabhan AN, Penland L, et al. A molecular cell atlas of the human lung from single-cell RNA
525 sequencing. Nature **2020**; 587:619-25.
526 23. Herta T, Bhattacharyya A, Bollensdorf C, et al. DNA-release by Streptococcus pneumoniae autolysin LytA
527 induced Krueppel-like factor 4 expression in macrophages. Sci Rep **2018**; 8:5723.
528 24. Barutcu AR, Lajoie BR, Fritz AJ, et al. SMARCA4 regulates gene expression and higher-order chromatin
529 structure in proliferating mammary epithelial cells. Genome Res **2016**; 26:1188-201.
530 25. Wilson R, Cohen JM, Jose RJ, de Vogel C, Baxendale H, Brown JS. Protection against Streptococcus
531 pneumoniae lung infection after nasopharyngeal colonization requires both humoral and cellular immune
532 responses. Mucosal Immunol **2015**; 8:627-39.
533 26. Periselneris J, Ercoli G, Pollard T, et al. Relative Contributions of Extracellular and Internalized Bacteria to
534 Early Macrophage Proinflammatory Responses to Streptococcus pneumoniae. mBio **2019**; 10.
535 27. Galan JE. Salmonella Typhimurium and inflammation: a pathogen-centric affair. Nat Rev Microbiol **2021**;
536 19:716-25.
537 28. Li G, Wang G, Li M, et al. Morin inhibits Listeria monocytogenes virulence in vivo and in vitro by targeting
538 listeriolysin O and inflammation. BMC Microbiol **2020**; 20:112.
539 29. Connor V, German E, Pojar S, et al. Hands are vehicles for transmission of Streptococcus pneumoniae in
540 novel controlled human infection study. Eur Respir J **2018**; 52:1800599.
541 30. Browall S, Norman M, Tangrot J, et al. Intraclonal variations among Streptococcus pneumoniae isolates
542 influence the likelihood of invasive disease in children. J Infect Dis **2014**; 209:377-88.
543 31. Love MI, Huber W, Anders S. Moderated estimation of fold change and dispersion for RNA-seq data with
544 DESeq2. Genome Biol **2014**; 15:550.
545 32. Yu G, Wang LG, Han Y, He QY. clusterProfiler: an R package for comparing biological themes among gene
546 clusters. OMICS **2012**; 16:284-7.
547 33. Rheinwald JG, Green H. Serial cultivation of strains of human epidermal keratinocytes: the formation of
548 keratinizing colonies from single cells. Cell **1975**; 6:331-43.

549 34. Carpenter AE, Jones TR, Lamprecht MR, et al. CellProfiler: image analysis software for identifying and
550 quantifying cell phenotypes. Genome Biol **2006**; 7:R100.
551 35. Kirkham LA, Kerr AR, Douce GR, et al. Construction and immunological characterization of a novel
552 nontoxic protective pneumolysin mutant for use in future pneumococcal vaccines. Infect Immun **2006**;
553 74:586-93.

554

555

556

557 **FIGURE LEGENDS**

558

559 **Fig 1. Pneumococcal – epithelial interactions in the EHPC model**. (A) Schematic showing that
560 during colonisation, pneumococci adhere to the epithelial cell surface (association), internalise inside
561 epithelial cells (microinvasion). Mucus – lime; pneumococci – purple; intracellular vacuole – dark
562 green; epithelial cells – yellow; nucleus – brown; cell junctions – pink. (B) Representative microscopy
563 images showing pneumococcal-epithelial interactions by the 6B WT, Δ*proABC/piaA* or Δ*fhs/piaA*
564 mutants. Surface carbohydrates (red), nuclei (DAPI, blue), pneumococci (green). (C) Table
565 summarising the microscopy and microbiology counts for each inoculated strain 6 days post
566 challenge per volunteer. Adherent represents pneumococcal surface association and intracellular
567 represents pneumococci that have microinvaded (inside) epithelial cells.

568

569 **Fig 2. Impact of pneumococcal infection on NHBE-A cell junctional protein expression and**
570 **barrier integrity.** NHBE-A Cells were cultured at ALI and infected with pneumococcal strains for
571 6hrs. (A) Top: Representative confocal microscopy images from 4 independent experiments with
572 replicates, showing pneumococcal (green) association with the epithelium (red, surface
573 carbohydrates; nuclei blue) at 6hr post infection. Bottom: Representative transmission electron
574 microscopy images from 2 independent experiments, showing pneumococcal microinvasion
575 examples of each strain (arrows), enclosed within a vacuole after 4hr infection. Representative
576 confocal microscopy images from four independent experiments with replicates showing
577 pneumococcal (green) interactions with junctional proteins (red); JAM-A (B), ZO-1 (C) and β catenin
578 (D) in primary HBE-A cells after a 6hr exposure. Nuclei stained with DAPI in blue. Co-localisation of
579 junctional proteins and pneumococci appear yellow, as highlighted by arrows. Integrated intensity of
580 β catenin in pneumococcal negative (not pneumococcal associated) or positive (pneumococcal
581 associated) cells. Non infected v pneumococcal negative cells **** p <0.0001 (NI v Δ*proABC/piaA*),
582 ** p = 0.0026 (NI v Δ*fhs/piaA*); non-infected v pneumococcal positive cells; **** p <0.0001 (NI v
583 Δ*proABC/piaA* and NI v Δ*fhs/piaA*); Kruskal-Wallis, n = 4 independent experiments.

584

585 **Fig 3. Pneumococcal – epithelial interactions with** NHBE-A**.** Cells were cultured at ALI and
586 infected with pneumococcal strains for 6hrs. (A) Representative scanning electron microscopy
587 images from 2 independent experiments, showing the surface of the epithelium. Representative
588 examples of differentiated epithelia (basal cells, Clara cells, goblet cells, ciliated cells) are shown in
589 yellow text. Colonising pneumococci are highlighted by arrows. Representative confocal microscopy
590 images from 4 independent experiments with replicates for (B) Ciliated cells (acetylated tubulin, red),
591 (C) Goblet cells (mucin5ac, red, (arrows indicate co-localisation of mucin5ac with pneumococci)),
592 (D) Clara cells (uteroglobin, red) after 6hr infection. Pneumococci (green), nuclei (DAPI, blue),
593 colocalization of red and green appears as yellow. Integrated intensity of acetylated tubulin (B) or
594 Muc5ac (C) in pneumococcal negative or positive cells from two or more images. Acetylated tubulin,
595 neg p = 0.2677, pos p = 0.017, ANOVA. Mucin5ac, neg p = 0.6852, pos p = 0.8510, N = 3 or 4
596 independent experiments. (D) Integrated intensity of uteroglobin normalised to non-infected cells
597 (left, p = 0.0115 non-infected v infected, Kruskal-Wallis) and percentage of Clara positive cells
598 following infection (right, p = 0.0003 non-infected v strains, p = 0.0036 6B v mutant strains, Kruskal-
599 Wallis). N = 3 independent experiments.

600

601 **Fig 4**. **Strain association, microinvasion and transmigration of Detroit 562 cells.** Cells were
602 infected with *S. pneumoniae* for three hours and CFU counts recorded. (A) Representative confocal
603 microscopy images from 6 independent experiments with replicates, showing pneumococcal (green)
604 interactions with surface carbohydrates (red). (B, top left) Association of pneumococcal strains to
605 epithelial cells. p = 0.0009 (Kruskal-Wallis), n = 6 with replicates. (B, top right) Internalisation of
606 strains into cells, following a gentamicin protection assay. p = 0.0219 (Kruskal-Wallis) N = 6 with
607 replicates. (B, bottom left) Pneumococcal viability inside epithelial cells following a gentamicin
608 protection assay. n = 3 or 4 independent experiments with replicates. Counts were normalised to
609 microinvasion counts for each strain after 3 hours infection and compared to 6B WT; +1hr p = 0.6517,
610 +2hr p = 0.1377, +3hr p = 0.1183 (ANOVA). (B, bottom right) Transmigration of pneumococcal
611 strains across confluent monolayers on transwell inserts. CFUs were recorded from the basal

612 chamber. N = 6 independent experiments with replicates. $p < 0.001$ (Kruskal-Wallis). (C)
613 Representative confocal microscopy images from 6 independent experiments with replicates,
614 showing pneumococcal (green) interactions with β catenin (red). Nuclear DAPI stain (blue).

615

616 **Fig 5. Detroit 562 cell transcriptomic responses to pneumococcal strains.** Epithelial cells were
617 infected for four hours with pneumococcal strains and RNA extracted and processed for RNAseq.
618 6B n = 11, PP n = 17, FP n = 14, non-infected n = 12, from 6 independent experiments. (A) All
619 significantly log2 fold change upregulated genes according to strain compared to non-infected cells.
620 Significance was defined as DEGs with a log2 fold change (logFC) of > 1.5 and false discovery rate
621 (FDR) of < 0.05. (B) Comparison of the top 20 most upregulated genes for each strain, compared to
622 non-infected cells. Upstream regulator analysis for (C) transcription factors and (D) kinases.

623

624 **Fig 6. Effects of pneumococcal infection on caspase activity in Detroit 562 cells.** Caspase
625 activity was assessed by luminescence, following infection with pneumococcal strains for 6 hours.
626 (A) Caspase 3/7 activity was determined following incubation with the specific inhibitor Z-VAD-FMK.
627 N = 4 with replicates. In comparison to non-infected cells, caspase 3/7 $p = 0.0022$; caspase 3/7 + Z-
628 VAD-FMK inhibitor $p = 0.0005$. In comparison to 6B WT, caspase 3/7 $p = 0.0215$; caspase 3/7 + Z-
629 VAD-FMK inhibitor $p = 0.0012$ (Kruskal-Wallis). (B) Caspase 1 activity was determined following
630 incubation with the specific inhibitor YVAD-CHO. Negative signals indicate caspase activity other
631 than caspase 1. N = 6 with replicates. In comparison to non-infected cells, $p = 0.39$; caspase+YVAD-
632 CHO inhibitor $p = 0.3604$ and, in comparison to 6B WT, $p = 0.6226$; caspase+YVAD-CHO inhibitor
633 $p = 0.5386$ (Kruskal-Wallis). (C) Caspase 8 activity was assessed following infection with
634 pneumococcal strains. N = 3 with replicates. In comparison to non-infected cells, $p = 0.0015$
635 (ANOVA) and, in comparison to 6B WT, $p = 0.0172$ (ANOVA).

636

637 **Fig 7. Hydrogen peroxide secretion and pneumolysin activity from pneumococcal strains in**
638 **the absence and presence of Detroit 562 cells. (**A) Fold change of hydrogen peroxide production

639 from the mutants compared to WT, normalised to the CFU counts. 3hr p = 0.0087 (ANOVA), 6hr p
640 = 0.0209 (Kruskal-Wallis). (B) Fold change of hydrogen peroxide production from the mutants
641 compared to WT, normalised to the CFU counts, following infection of Detroit 562 cells. Media was
642 replaced after 1hr infection and cells incubated for a further 5hrs. N = 3 independent experiments
643 with replicates. Compared to 6B WT, p = 0.0034 (ANOVA). (C) Pneumolysin activity was assessed
644 using a red blood cell lysis assay. Strains were incubated with red blood cells for 30 minutes and
645 absorbance measured. N = 4 experiments with replicates. Pneumococcal strain haemolytic activity
646 is calculated in comparison to 100% lysis by 0.0625% saponin. p <0.0001 compared to 6B WT
647 (ANOVA).

Figure 1. Pneumococcal – epithelial interactions in the EHPC model

A

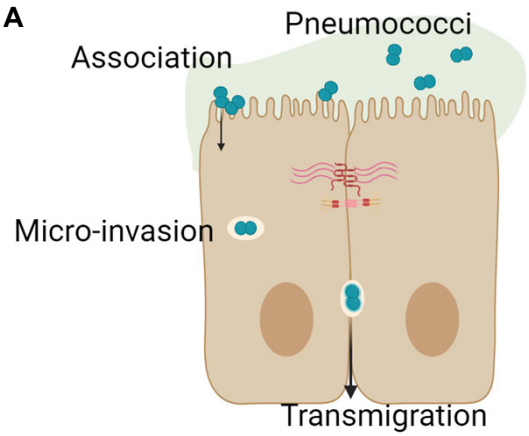

B

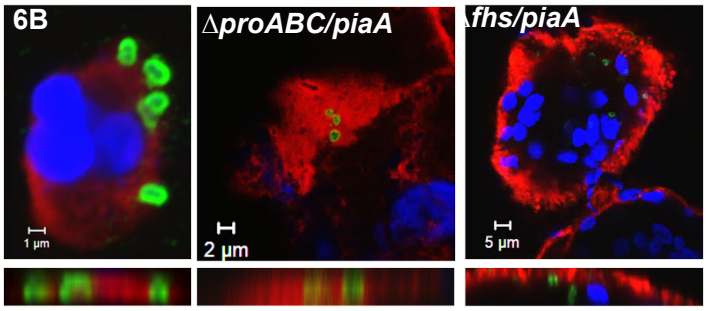

C

6B	MICROSCOPY		MICROBIOLOGY
	Adherent	Intracellular	
#1	0	0	0
#2	2	0	520
#3	0	0	0
#4	1	0	0
#5	0	0	9
#6	1	2	223
#7	0	0	5725
#8	39	4	1110
#9	0	0	0
#10	0	0	767
#11	0	0	0

Δ*proABC/piaA*	MICROSCOPY		MICROBIOLOGY
	Adherent	Intracellular	
#1	0	0	0
#2	0	0	0
#3	0	0	0
#4	5	3	0
#5	3	2	0
#6	8	2	5
#7	0	0	0
#8	0	2	0
#9	0	2	1
#10	0	0	0
#11	0	0	0

Δ*fhs/piaA*	MICROSCOPY		MICROBIOLOGY
	Adherent	Intracellular	
#1	2	0	21856
#2	1	3	0
#3	3	3	16
#4	51	54	0
#5	0	0	520325

Figure 2. Impact of pneumococcal infection on NHBE-A cell junctional protein expression and barrier integrity.

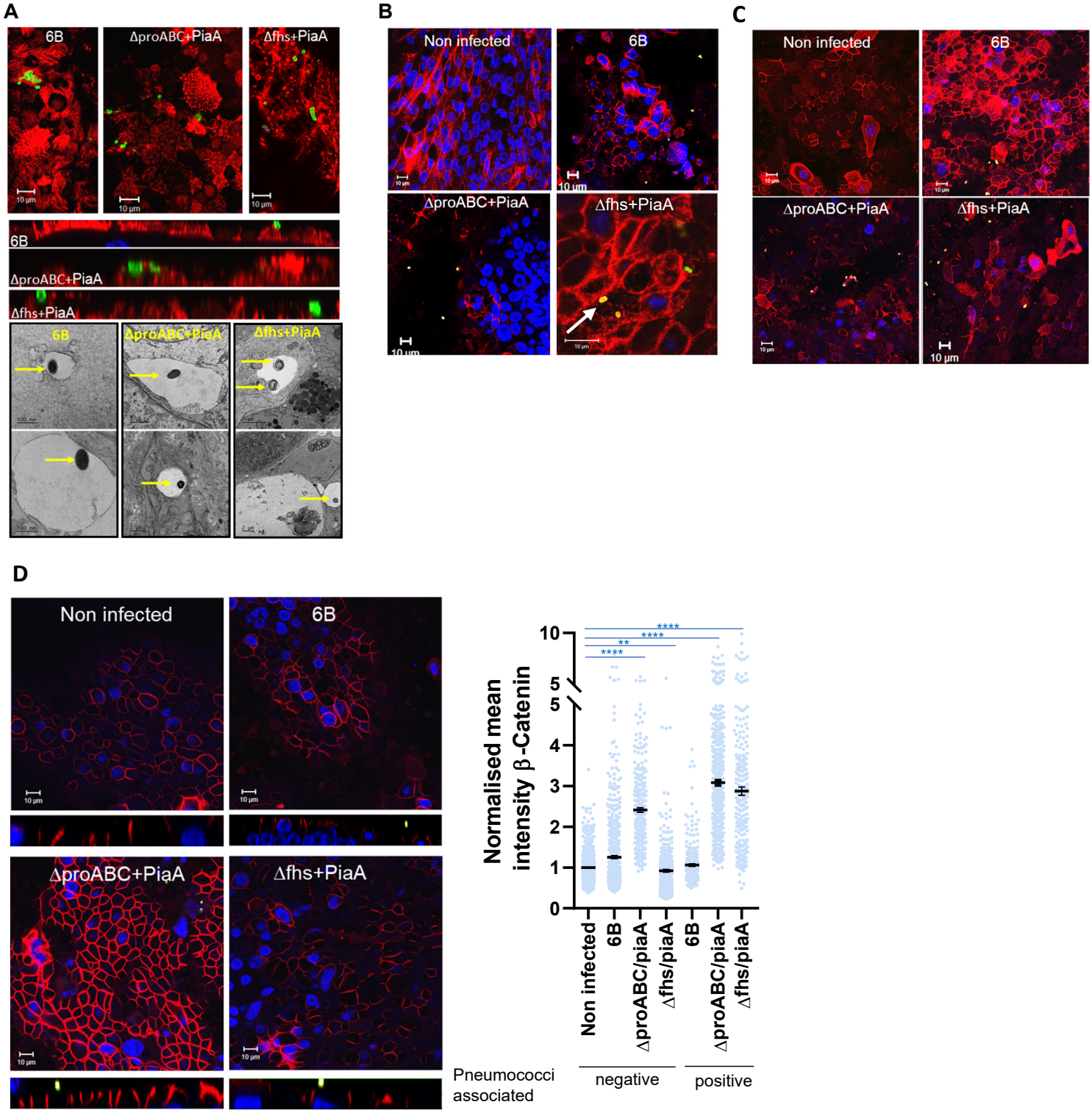

Figure 3. Pneumococcal – epithelial interactions with primary human epithelial cells.

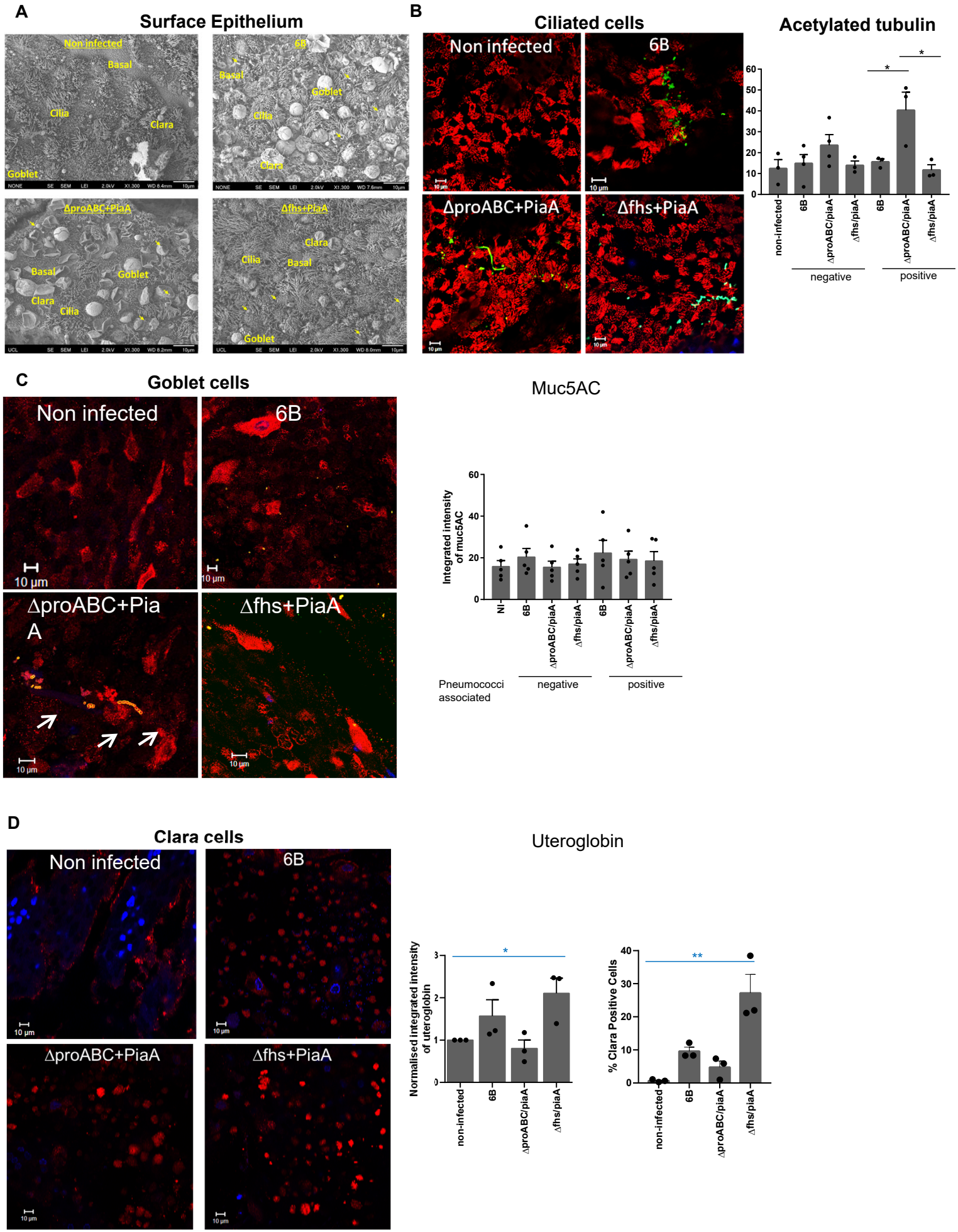

Figure 4. Strain association, microinvasion and transmigration of Detroit 562 cells.

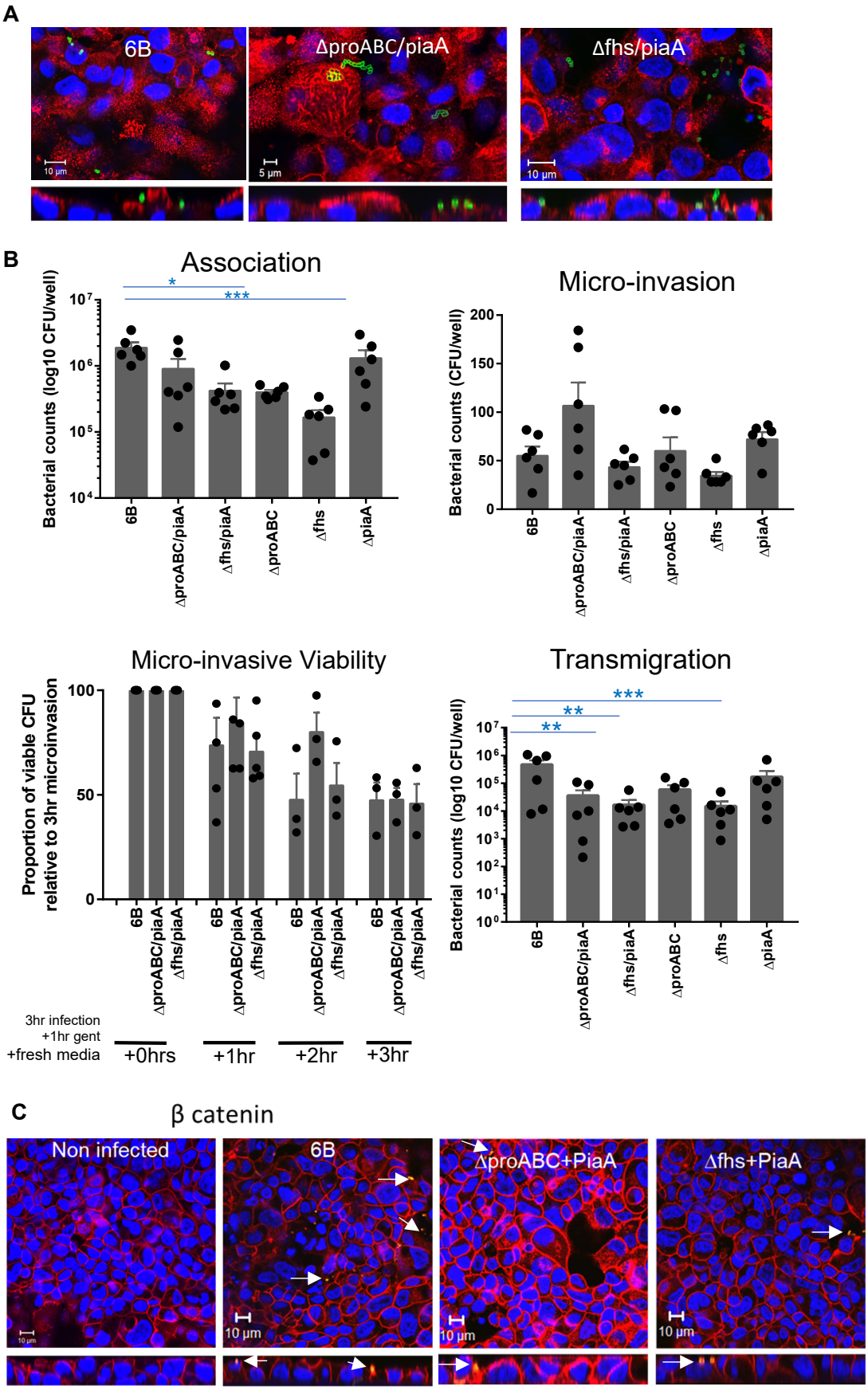

Figure 5. Detroit 562 cell transcriptomic responses to pneumococcal strains.

A

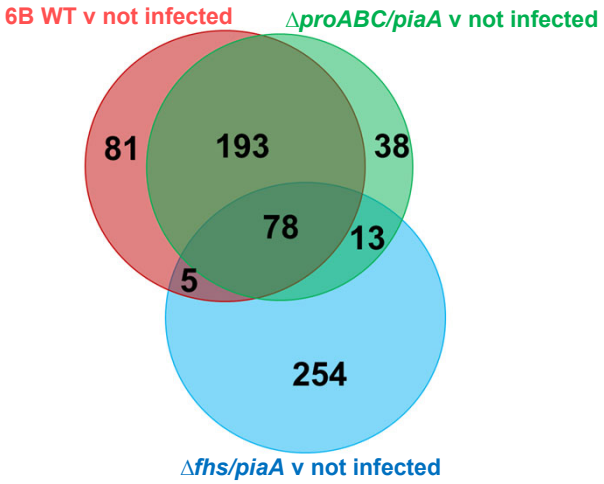

B

log2foldchange	6B	ΔproABC/piaA	Δfhs/piaA
Upregulated genes			
AC256236.1	32.9	25.5	0.0
AC022149.1	30.2	27.6	0.0
Z84488.2	29.1	21.6	0.0
MUC21	25.8	29.0	0.0
VASN	20.9	0.0	0.0
BRD2	18.4	24.7	0.0
AC012254.2	18.2	13.8	0.0
CTAGE4	18.1	0.0	0.0
MICE	17.1	20.3	0.0
AC107075.1	10.1	0.0	0.0
CSNK2B	0.0	20.2	0.0
MTRNR2L6	0.0	19.4	15.8
LSM2	0.0	17.1	0.0
ALOX5	0.0	0.0	6.9
AC006064.6	0.0	0.0	3.4
TAP2	0.0	0.0	3.2
CYP1A1	0.0	0.0	1.7
FOSB	0.0	0.0	1.4
IL1B	0.0	0.0	1.3
CXCL8	0.0	0.0	1.1
CXCL2	0.0	0.0	1.1
CYP1B1	0.0	0.0	1.0

C

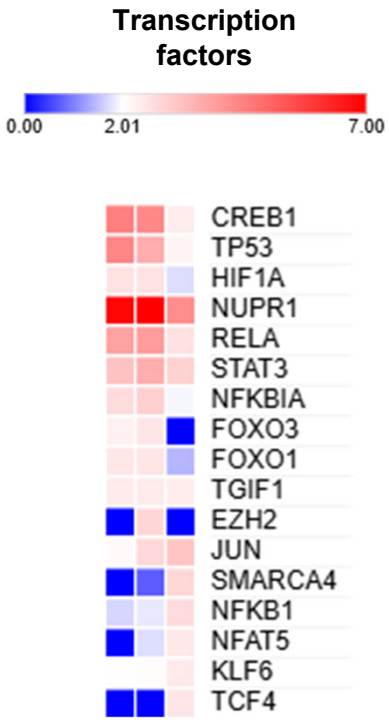

D

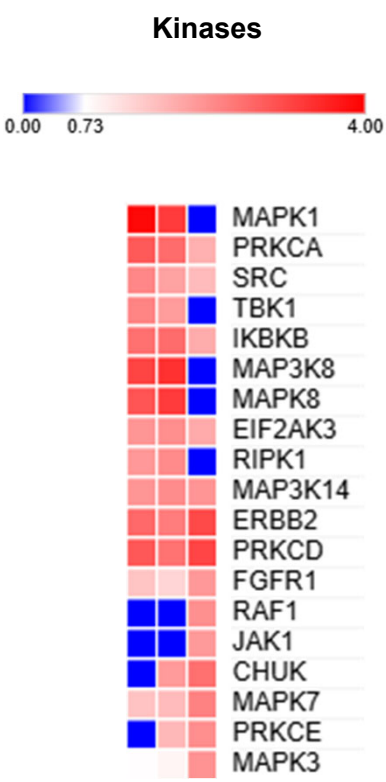

Figure 6. Effects of pneumococcal infection on caspase activity in Detroit 562 cells.

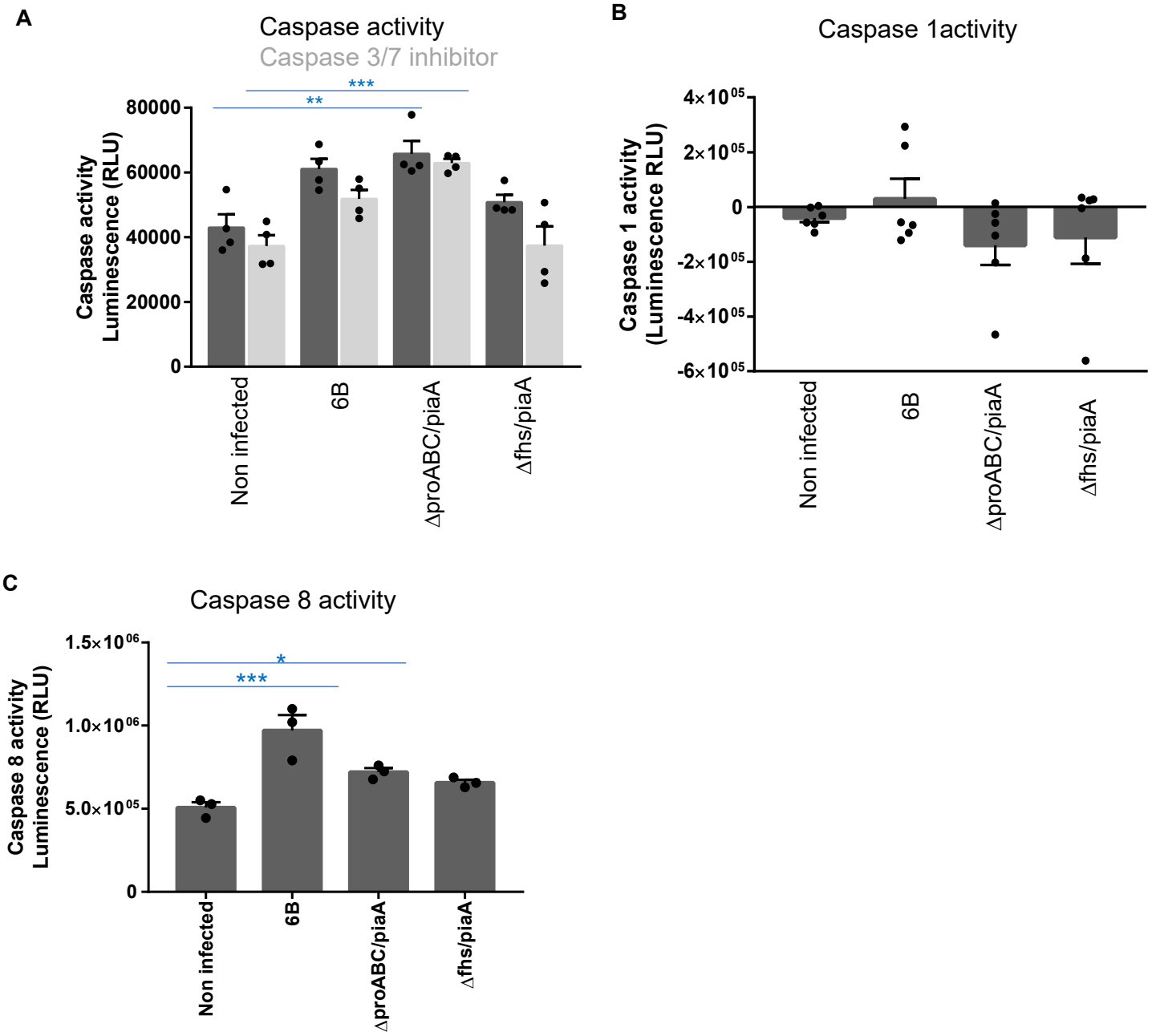

Figure 7. Hydrogen peroxide secretion and pneumolysin activity from pneumococcal strains in the absence and presence of Detroit 562 cells.

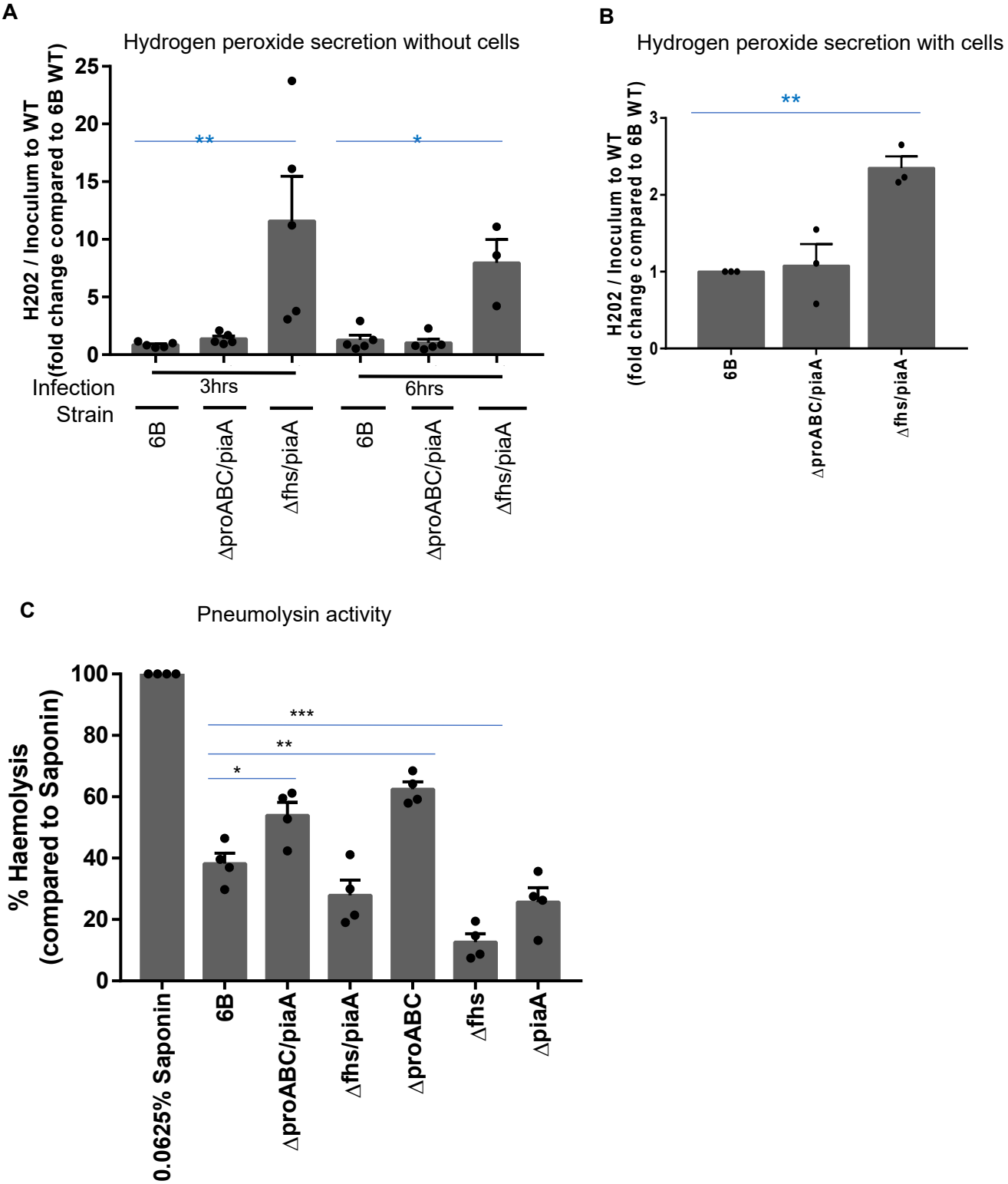
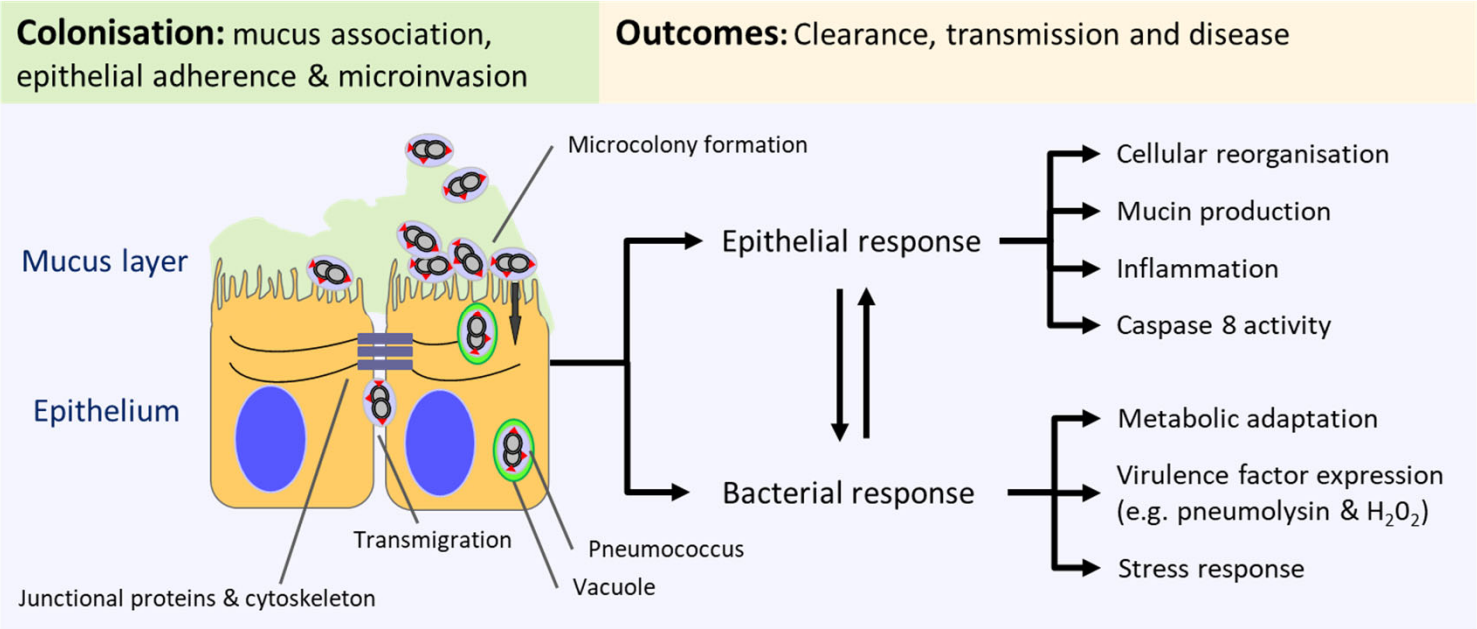
Graphical abstract